Surface damage and structure evolution of recrystallized tungsten exposed to ELM-like transient loads

2016 Nucl. Fusion 56 036021

(http://iopscience.iop.org/0029-5515/56/3/036021)

IOP Publishing | International Atomic Energy Agency Nuclear Fusion

Nucl. Fusion **56** (2016) 036021 (8pp) doi:10.1088/0029-5515/56/3/036021

Surface damage and structure evolution of recrystallized tungsten exposed to ELM-like transient loads

Y. Yuan[1], J. Du[2], M. Wirtz[2], G.-N. Luo[3], G.-H. Lu[1] and W. Liu[4]

[1] School of Physics and Nuclear Energy Engineering, Beihang University, Beijing 100191, People's Republic of China
[2] Forschungszentrum Jülich, Institut für Energie- und Klimaforschung, 52425 Jülich, Germany
[3] Institute of Plasma Physics, Chinese Academy of Sciences, Hefei, Anhui 230031, People's Republic of China
[4] School of Material Science and Engineering, Tsinghua University, Beijing 100084, People's Republic of China

E-mail: yueyuan@buaa.edu.cn and liuw@mail.tsinghua.edu.cn

Received 5 October 2015, revised 13 January 2016
Accepted for publication 19 January 2016
Published 19 February 2016

Abstract

Surface damage and structure evolution of the full tungsten ITER divertor under transient heat loads is a key concern for component lifetime and plasma operations. Recrystallization caused by transients and steady-state heat loads can lead to degradation of the material properties and is therefore one of the most serious issues for tungsten armor. In order to investigate the thermal response of the recrystallized tungsten under edge localized mode-like transient thermal loads, fully recrystallized tungsten samples with different average grain sizes are exposed to cyclic thermal shocks in the electron beam facility JUDITH 1. The results indicate that not only does the microstructure change due to recrystallization, but that the surface residual stress induced by mechanical polishing strongly influences the surface cracking behavior. The stress-free surface prepared by electro-polishing is shown to be more resistant to cracking than the mechanically polished one. The resulting surface roughness depends largely on the loading conditions instead of the recrystallized-grain size. As the base temperature increases from room temperature to 400 °C, surface roughening mainly due to the shear bands in each grain becomes more pronounced, and sub-grains (up to 3 μm) are simultaneously formed in the sub-surface. The directions of the shear bands exhibit strong grain-orientation dependence, and they are generally aligned with the traces of $\{1\,1\,2\}$ twin habit planes. The results suggest that twinning deformation and dynamic recrystallization represent the predominant mechanism for surface roughening and related microstructure evolution.

Keywords: tungsten, surface damage, structure evolution, transient heat loads

(Some figures may appear in colour only in the online journal)

1. Introduction

Transient heat loads, which typically occur as a result of edge-localized modes (ELMs), vertical displacement events (VDEs) and disruptions, are expected to be the predominant threat to the power handling capability and lifetime of the full tungsten (W) ITER divertor [1]. ELMs have invariably been a critical concern in view of plasma-facing material (PFM) damage [2, 3]. ELMs are predicted to repeatedly deposit power densities up to 1 GW m^{-2} onto the divertor surface for 0.1–0.5 ms, inducing a sharp temperature gradient and a high thermal stress. Owing to the intrinsic brittleness and high ductile-brittle transition temperature (DBTT), W-PFMs readily crack under this strong cyclic thermal stress.

Considerable research [4–7] has been focused on the macroscopic damage of W materials under ELM-like thermal shock loads. The results indicate that the thermal response strongly depends on the microstructure, which closely correlates not only with the production process, but with the exposure history. Rolled W quickly recrystallizes and the grains grow noticeably larger under adiabatically VDE-like short pulse high heat flux (HHF) loading [8]. The recrystallized W will further face ELM-like transient heat loads. This provides motivation for the investigation of the behavior of recrystallized W under ELM-like heat loads.

In order to investigate W behavior under expected transient thermal loads, using dedicated transient loading (e.g. electron beams, lasers and quasi-stationary plasma accelerators) is a cost-effective and flexible approach. Several critical loading parameters (such as base temperature, power density and cycle number) linked to the brittle/ductile state of the bulk W and the accumulated thermal stress/strain state are normally taken into account [6, 7, 9]. Recently, the transient peak temperature and the temporal pulse shape have been found to have an important impact on the surface damage [10, 11]. However, the surface residual stress induced during the sample preparation process, e.g. grinding and mechanical polishing [12, 13], has been largely neglected. So far, it is not very clear what role the surface polishing technique plays in the surface cracking behavior under transient thermal shocks.

Compared to surface cracking, surface roughening is observed to be a more common damage feature on the loaded surface, even if the heat loading is far below the cracking threshold. Surface roughening is influenced by the peak surface temperature, pulse shape, power density, base temperature, etc [9–11, 14, 15], and it features shear bands that appear on the grain surface. The shear bands are described as a form of plastic deformation, but the detailed deformation mechanism and the related microstructure evolution have as yet hardly been discussed.

In this work, we expose recrystallized W to ELM-like thermal shocks and investigate both surface cracking and roughening behavior. We assess the cracking resistance by comparing the recrystallized W and the original rolled W in different test conditions. Meanwhile, the impact of the surface state introduced by different surface preparation methods is considered. As for surface roughening, besides the evolution of surface roughness with varying recrystallized-grain size and loading conditions, we focus on the potential mechanism of surface deformation (typically the shear bands) and related microstructure evolution.

2. Experimental

Fully recrystallized W plate was obtained by applying VDE-like short pulse heat loads onto commercially rolled W plate (75% thickness reduction, grain size ~5 μm) in the HHF test facility GLADIS at IPP-Garching [8, 16]. For the ELM-like thermal shock tests, small samples of $12 \times 12 \times 3\,\mathrm{mm}^3$ with four different average grain sizes of 25, 50, 75 and 100 μm (analyzed by electron back-scattering diffraction (EBSD)) were cut from the recrystallized W plate. As a reference, commercially rolled W with the elongated grains perpendicular to the heat loading direction was also tested.

The surface of the sample was first ground to an average surface roughness (R_a) of ~0.3 μm. Afterwards, two different methods were used for surface finishing: mechanical polishing by diamond paste with a particle size down to 1 μm, and electro-polishing in a 2 wt. % NaOH solution for >1 min, which removed the distortion layer and produced a stress-free surface. The final surface roughness after the two polishing processes was measured to be similar ($R_a < 0.1$ μm). Therefore, the main difference between the mechanical and electro-polished surfaces was the surface stress state.

ELM-like transient heat loading tests were performed in the electron beam facility JUDITH 1. Before exposure, the samples were either kept at room temperature (RT) or pre-heated to 400 °C. The electron beam had the energy of 120 keV and caused volumetric loading with a penetration depth of 5–10 μm [17]. Homogenous loading was achieved on the $4 \times 4\,\mathrm{mm}^2$ loading area using the fast scanning beam (with a frequency of 47 kHz in the x-direction and 43 kHz in the y-direction) with a beam diameter of c.a. 1 mm. The incident current through the loaded sample was measured to be 92 and 275 mA, and the absorbed power densities were 0.38 and 1.14 GW m^{-2}, respectively (the electron absorption coefficient of W is 0.55). The samples were subjected to 100 cycles of pulses with a duration of 1 ms and followed by an inter-pulse duration of 2–3 s to ensure a complete cooling of the loaded surface to the base temperature. The evolution of the maximum temperature on the loaded area during and after a pulsed loading at RT was simulated by finite element methods (FEMs) [18].

After the cyclic thermal shock tests, the surface profile was observed by a confocal laser scanning microscope (CLSM). The surface roughness (R_a) was obtained by scanning an area of 2560×2560 μm, which covered the major loaded area, with a step-length of 2.5 μm. The surface morphology and microstructure were investigated using a scanning electron microscope (SEM), including backscatter electron imaging (BEI) and EBSD. The BEI mode in SEM is useful for the observation of sub-surface structures. The variation in the backscattered electron (BSE) signal intensity with the crystallographic orientation enables mapping of deformation and misorientation boundaries within the coarse recrystallized grains [19]. EBSD and trace analysis were used to identify the crystallographic orientation characteristic of the shear bands [20]. The grain orientation was determined by EBSD indexing and the inclination angle of the shear bands to the sample axis was measured from the SEM image. The crystallographic indexes of the shear bands were then calculated based on the geometrical relationship [21]. For the detailed observation of the cross-section of the near surface, a focused ion beam (FIB) was implemented.

3. Results and discussion

3.1. Thermal shock cracking resistance

Table 1 summarizes the cracking response of rolled and recrystallized W samples prepared by mechanical and electro-polishing after exposure to 100 pulses of 1.14 GW m^{-2} at RT

Table 1. Cracking response after exposure to 100 thermal shocks of 1.14 GW m^{-2} at different base temperatures.

	Electro-polishing		Mechanical polishing	
State	RT	400 °C	RT	400 °C
Rolled	No cracking	No cracking	No cracking	No cracking
Recrystallized	No cracking	No cracking	Cracking	No cracking

and 400 °C. For each test, one sample was used. No cracks appeared in any of the rolled W samples, indicating the cracking threshold is above 1.14 GW m^{-2} for 100 pulses. This is significantly higher than for the other grades of deformed W, e.g. single forged ultra-high-purity W (>99.9999%) and ITER-grade W, which were tested with similar loading conditions in other studies [5, 9, 22, 23].

For the recrystallized W, it should be noted that four samples with an average grain size of 50 μm were selected as representative for demonstrating the effect of recrystallization on the cracking resistance. As seen in table 1, only the mechanically polished sample that was loaded at RT cracked. That is to say, the base temperature and surface preparation method both influence the cracking resistance.

It is well known that W, as a body-centered cubic (bcc) metal, is more brittle at lower temperatures, especially below DBTT [24]. Accordingly, W tends to crack more easily at RT than at 400 °C. The fact that the recrystallized W sample cracked at RT, while the rolled one did not, indicates that recrystallization reduces the cracking resistance [14, 15, 23, 25]. The cracking response is strongly linked to the microstructure and mechanical properties [5, 22, 23]. Dislocation annihilation, boundary migration and grain growth during recrystallization result in lower mechanical strength and a degraded ability to hinder crack formation and propagation [23, 24, 26].

Figure 1 illustrates the surface morphology of the mechanically and electro-polished recrystallized W (average grain size of 50 μm) before and after 100 pulses of 1.14 GW m^{-2} at RT. As seen in figures 1(*a*) and (*b*), mechanical polishing results in many fine scratches and pits on the surface, while the grains/etched grain boundaries can be clearly seen after electro-polishing. After transient heat loads, the mechanically polished sample was severely damaged (figure 1(*c*)). Open cracks indicate that cracking is induced by tensile stresses ascribed to volumetric shrinkage during the cooling process [22]. In contrast, no cracks were found for the sample prepared by electro-polishing (figure 1(*d*)). The cracking pattern in the mechanically polished surface (figure 1(*c*)) shows that the cracks initiated at the center of the loading area and spread radially to the edge. Since the microstructure of the fully recrystallized W is homogeneous [8], the radial cracking pattern could be mainly due to uneven stress distribution on the surface. Although the rolling deformation can induce large internal stresses, they can be completely released after full recrystallization [26]. Therefore, for the loaded recrystallized W, the stress distribution largely depends on the thermo-stress resulting from the transient heat load and the surface residual stress introduced by mechanical polishing. As mentioned in section 2, fast scanning of the electron beam produced an homogeneous heat load, and in principle, a uniform thermo-stress distribution on the exposed surface was expected. Therefore, we speculate that the uneven stress distribution mainly resulted from the surface residual stress caused by mechanical polishing.

Compared to mechanical polishing, the main contribution of electro-polishing is the removal of the surface deformation layer. The key benefit [27–29] is that the residual stress layer is almost eliminated and replaced by a stress-less surface, and thus may alleviate the cracking initiation and propagation.

However, the influence of the surface polishing method on the cracking behavior is not clarified, as only one sample was used for each test in this work. The results (figure 1) suggest a lower cracking threshold for the mechanically polished surface compared to the electro-polished surface. More thermal shock tests and quantitative analyses on the cracking behavior under single and multiple transient thermal shocks will be performed in the future.

Since the cracking threshold of the investigated rolled W is quite high, no cracks were formed on either kind of surface in the present work (table 1). Due to the higher cracking threshold of the rolled W than the recrystallized W, the impact of the surface residual stress on the cracking threshold would not be as significant as that for the recrystallized W.

3.2. Surface roughness

Since no cracks formed in the recrystallized W samples with stress-free surfaces prepared by electro-polishing under the applied loading conditions, we further investigated surface roughening and related microstructure changes of these samples. As shown in figure 2, the roughness value is rarely affected by varying recrystallized-grain size, while it depends strongly on the loading conditions. It should be noted that no significant growth of the recrystallized grains was observed after any of the thermal shock tests in the present work.

The surface morphology of the recrystallized W with an average grain size of 50 μm exposed to two different power densities at RT and 400 °C is shown in figure 3. It can be found that surface roughening displays two main facets: bulging along grain boundaries, and the shear bands that appear in each grain. In principle, both of these are ascribed to the swelling of grain boundaries and the plastic deformation of the heated grains caused by compressive stress during heat loading [22]. According to the features of the two aforementioned facets of surface roughening on the loaded surfaces (figure 3), the density of the intragranular shear bands is higher than that of the grain boundaries, and it is weakly linked to the grain size. Consequently, the roughness remains at a consistent level for different recrystallized-grain sizes (25–100 μm) under a specific loading condition (figure 2).

As seen in figures 2 and 3, surface roughening became more significant when the base temperature was increased from RT to 400 °C for each power density. According to the stress–strain curves of recrystallized W [23], with the same stress state, higher plastic strain occurs at a higher base temperature. In the present study, when the sample was loaded with the same power density, it was reasonable that stronger

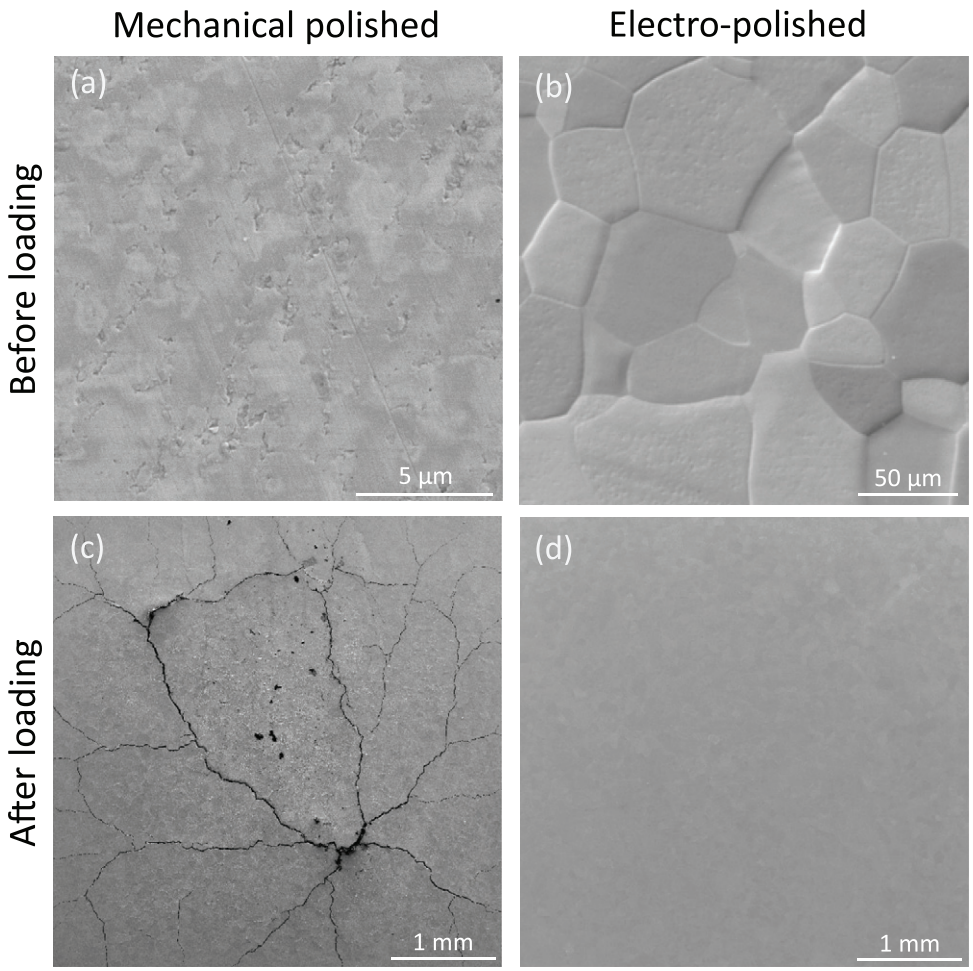

Figure 1. Surface morphology of the recrystallized W (average grain size of 50 μm) prepared by mechanical polishing and electro-polishing, before and after exposure to 100 thermal shocks of 1.14 GW m^{-2} at RT.

deformation was produced at 400 °C than at RT (figures 3(*c*) and (*d*) versus (*a*) and (*b*)).

In addition, for each base temperature, with increasing power density, the surface roughness was found to increase (figures 2 and 3). Figure 4 shows the FEM calculated maximum temperatures of the samples loaded at RT with 0.38 and 1.14 GW m^{-2}, respectively. The peak temperature induced by the 1.14 GW m^{-2} loading is about three times higher than that induced by the 0.38 GW m^{-2} loading. For a specific base temperature (the same deformation capability), when the power density was increased from 0.38 to 1.14 GW m^{-2}, a higher peak temperature and a more severe stress state were induced at the loaded area. Therefore, a larger deformation should be generated (figures 3(*a*) and (*c*) versus (*b*) and (*d*)).

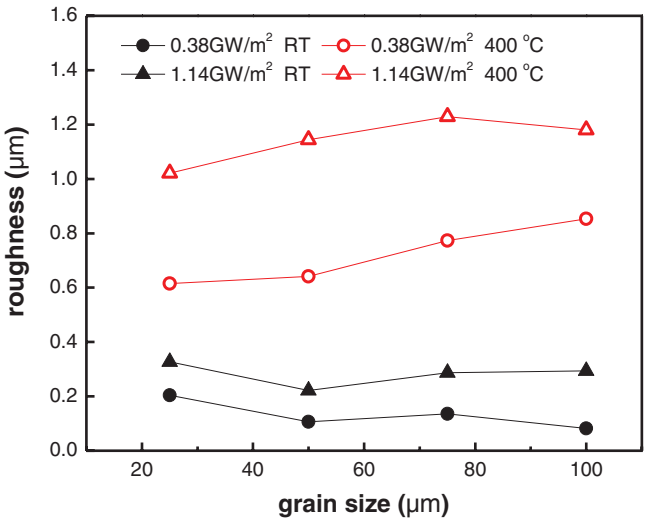

Figure 2. Surface roughness (R_a) of the electro-polished recrystallized W with different average grain sizes after 100 thermal shocks.

3.3. Microstructure evolution and potential mechanisms

The shear bands are aligned in different directions for varying grains (as in figures 3(*c*) and (*d*)), showing strong crystallographic orientation dependence. A typical roughened surface which was loaded by 100 thermal shocks of 1.14 GW m^{-2} at 400 °C is shown in Figure 5. 12 typical grains which have distinct shear patterns were selected. Table 2 illustrates the detailed information of these grains, including the grain orientation (Miller indexes) and the inclination angle of the shear bands/ the specific $\{1\,1\,2\}$ plane to the *x*-direction. It was found that the shear bands are parallel to the $\{1\,1\,2\}$ twin habit planes to within $\pm 5°$. The same relationship between the

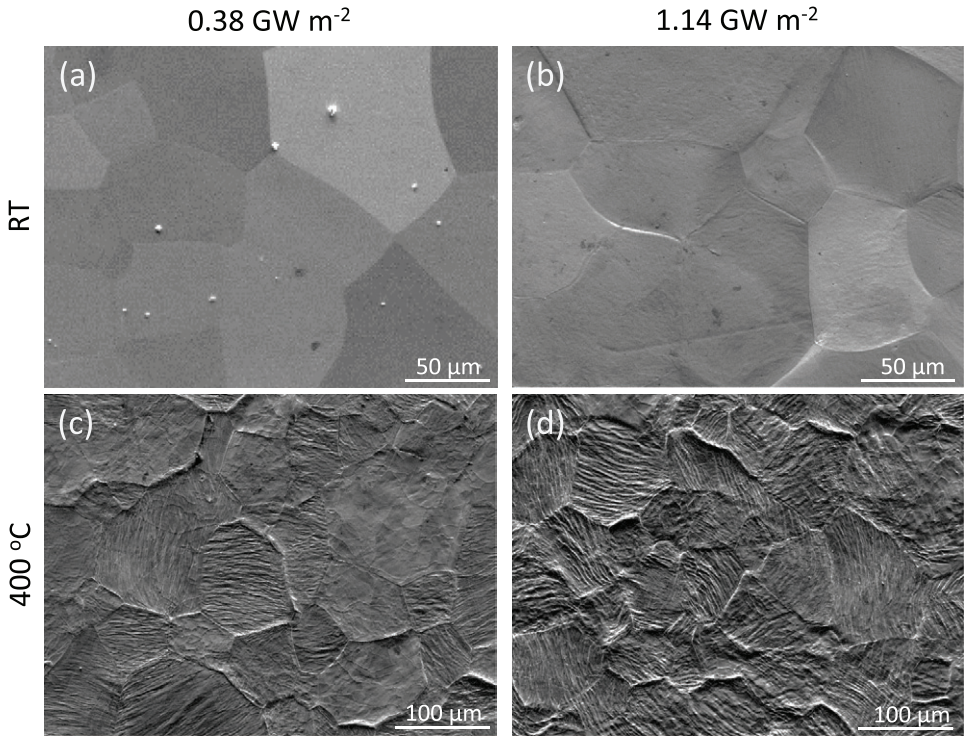

Figure 3. SEM images of the electro-polished recrystallized W (average grain size of 50 μm) after exposure to 100 thermal shocks of (*a*) 0.38 GW m^{-2} at room temperature, (*b*) 1.14 GW m^{-2} at room temperature, (*c*) 0.38 GW m^{-2} at 400 °C and (*d*) 1.14 GW m^{-2} at 400 °C.

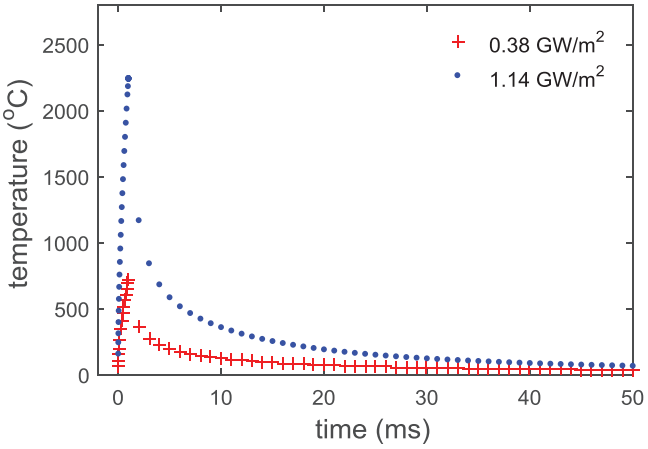

Figure 4. FEM simulation results of the maximum temperature evolution during and after a 1 ms pulsed loading at RT.

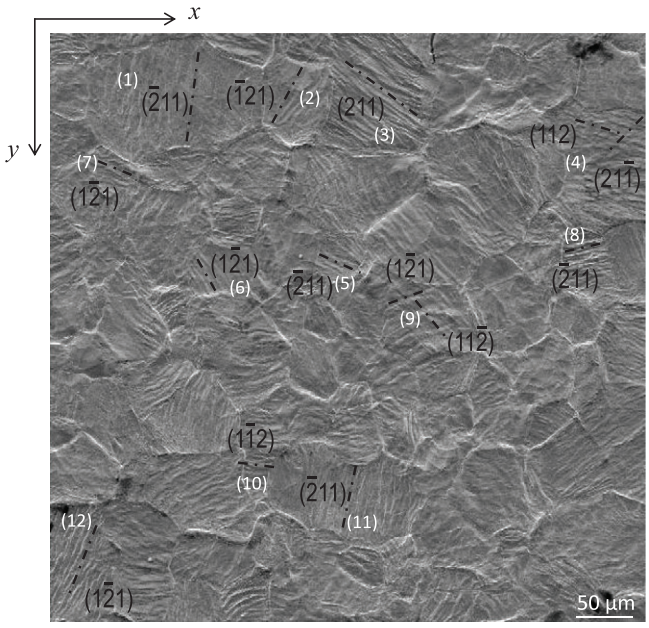

Figure 5. An SEM image of a typical roughened surface after 100 thermal shocks of 1.14 GW m^{-2} at 400 °C. 12 grains with distinct shear patterns are selected for the crystallographic orientation analysis of the shear bands (the bar above the crystallographic indexes denotes minus).

shear bands and the $\{1\,1\,2\}$ planes was also found on several other roughened surfaces involving around 50 grains.

Owing to the strain rate sensitivity of the flow stress in W, twinning and grain boundary de-cohesion are the favored deformation mechanisms under high strain rate conditions [30]. The occurrence of twinning deformation parallel to the $\{1\,1\,2\}$ habit planes has been commonly observed in bcc metals under shock loading [31–34]. A key feature of twinning deformation is the shape change resulting from a simple shear of the lattice points as a reflection in the twin plane [35]. As a result, overlapping shear bands are formed parallel to the twin plane on the deformed grain surface [31]. Accordingly, we conjecture that under transient thermal shocks, twinning deformation is a paramount approach for W materials to release the large thermo-stress, leading to the roughened surface with shear bands.

According to the BSE images shown in figure 6, little deformation was observed (uniform crystallographic contrast within grains) on the surface exposed to 0.38 GW m^{-2} at RT (figure 6(*a*)). When the power density increased to

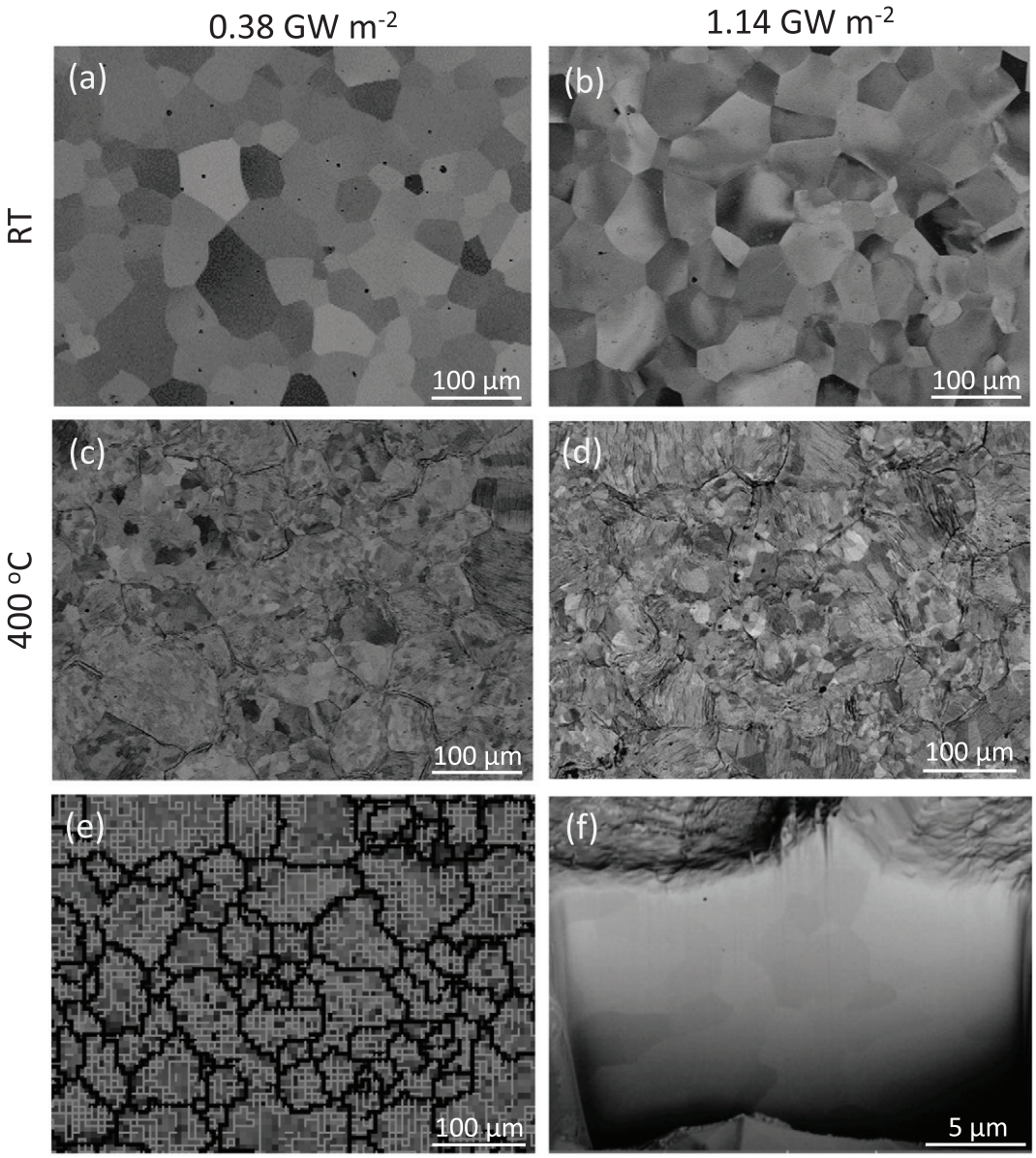

Figure 6. BSE images of the surface microstructures for recrystallized W after 100 thermal shocks with (*a*) 0.38 GW m^{-2} at RT, (*b*) 1.14 GW m^{-2} at RT, (*c*) 0.38 GW m^{-2} at 400 °C and (*d*) 1.14 GW m^{-2} at 400 °C. In addition, (*e*) is the EBSD map of (*d*), where the thick black lines represent misorientations more than 15° and the thin gray lines represent those in the range of 2–15°, and (*f*) is a BSE image of a local FIB cross-section of (*d*).

1.14 GW m^{-2}, crystallographic deformation characterized by varied contrast within the grains was observed (figure 6(*b*)). Nevertheless, for the samples loaded at 400 °C, a sub-grain structure was progressively formed (figures 6(*c*) and (*d*)). The EBSD image (figure 6(*e*)) indicates that the coarse recrystallized grain is divided into many small grains with misorientations of 2–15°. A BSE image of an FIB cross-section (figure 6(*f*)) shows that the equiaxed sub-grains (up to 3 μm) with uniform contrast and faceted boundaries extend to more than ~10 μm in depth.

The phenomenon essentially involving the development of a sub-grain structure with a low density of dislocations as a type of recrystallization during plastic deformation is known as dynamic recrystallization (DRX) [36]. As shown in figure 6, DRX occurred significantly when the base temperature was increased to 400 °C (figures 6(*c*) and (*d*)), where equiaxed sub-grains were noticeably formed as opposed to at RT (figures 6(*a*) and (*b*)). It indicates that DRX strongly depends on the base temperature. It is pronounced when the W bulk is in a relatively ductile state, which is susceptible to plastic deformation.

A greater propensity of DRX has been observed in a variety of cases of severe plastic deformation of metals and alloys, such as shock loading, ballistic impact and penetration, where a significant temperature excursion is generated in the adiabatic shear bands [36]. The nucleation mechanism for DRX under these extreme conditions can be described by a model of progressive sub-grain misorientation recrystallization [37], which is based on mechanically assisted sub-grain rotation. According to this model, the rotation of the sub-grains with

Table 2. The detailed information for the investigated grains indicated in figure 5, including the grain orientation and the inclination angle of the {1 1 2} habit planes/ the shear bands to the *x*-direction.

Grain No.	Miller indexes (*hkl*)[*uvw*]	{1 1 2} planes	The angle between the {1 1 2} plane and the *x*-direction (°)	The angle between the shear bands and the *x*-direction (°)
1	(1 2 2)[5 $\bar{1}$ $\bar{1}$]	($\bar{2}$ 1 1)	87	82
2	(1 1 2)[3 $\bar{1}$ $\bar{1}$]	($\bar{1}$ 2 1)	62	58
3	(1 5 5)[$\bar{2}$ 3 $\bar{2}$]	(2 1 1)	148	145
4	(5 1 5)[$\bar{2}$ $\bar{5}$ 3]	(1 1 2)	167	163
		(2 1 $\bar{1}$)	57	53
5	(1 3 3)[1 $\bar{3}$ 2]	($\bar{2}$ 1 1)	160	157
6	(2 1 3)[1 4 $\bar{2}$]	(1 $\bar{2}$ 1)	123	119
7	(2 1 2)[2 1 $\bar{2}$]	(1 $\bar{2}$ 1)	162	157
8	(1 4 4)[1 3 $\bar{3}$]	($\bar{2}$ 1 1)	13	10
9	(1 0 3)[$\bar{3}$ 0 1]	(1 $\bar{2}$ 1)	16	20
		(1 1 $\bar{2}$)	125	129
10	(3 1 4)[3 1 $\bar{2}$]	(1 $\bar{1}$ 2)	155	160
11	(1 4 4)[4 0 $\bar{1}$]	($\bar{2}$ 1 1)	80	78
12	(3 1 3)[$\bar{4}$ 7 1]	(1 $\bar{2}$ 1)	67	68

subsequent dislocation annihilation, which leads to the transformation of sub-grain dislocation walls to grain boundaries results in the reduction of dislocations and the formation of the fine DRX grains. In turn, this can facilitate the solid-state flow and promotes deformation by work softening due to the elimination of dislocation tangles and the rotation of the refined grains [38].

In this context, we can determine the mechanism concerning the noticeable morphology and microstructure changes at the base temperature of 400 °C (figures 3 and 6). Owing to the relatively ductile nature of W at elevated base temperature, the grains deformed under the cyclic transient thermal loading were associated with the formation of a considerable number of deformed sub-structures. These deformed sub-structures combined with the significant temperature rise during heat loading, triggered DRX, which in return enhanced further deformation and finally resulted in exaggerated plastic flow on the surface under multiple thermal shock loads.

4. Conclusion

The thermal response of the recrystallized W under ELM-like transient heat loads has been studied in the electron beam facility JUDITH 1. 100 pulses with power densities of 0.38 and 1.14 GW m^{-2} were applied at RT and 400 °C respectively. The effect of the surface preparation method on the surface cracking and the potential mechanism of surface roughening and related structure evolution are the main concerns of the present study.

The results indicate that not only microstructure changes due to recrystallization, but the surface residual stress induced by mechanical polishing can significantly affect the cracking formation. After full recrystallization, the cracking resistance is reduced. Moreover, the stress-free surface prepared by electro-polishing exhibits higher resistance to cracking formation compared to the mechanically polished surface. It is suggested that electro-polishing is a cost-effective and powerful approach to help targets survive cracking damage under transient thermal shocks, though more tests are needed.

Surface roughening and related microstructure evolution have been investigated, mainly based on the electro-polished samples without cracking damage. The average surface roughness exhibits a weak correlation with the recrystallized-grain size, while it is significantly affected by the loading conditions, e.g. base temperature and power density. Surface roughening, mainly due to the intragranular shear bands, is more pronounced at elevated base temperature and higher power density. The directions of the shear bands are found to be generally aligned with the traces of {1 1 2} twin habit planes, which implies that twinning may be one of the main deformation mechanisms of W materials under thermal shock loads. Significant DRX is also observed in the sub-surface after cyclic thermal shocks at elevated base temperature, which in turn can facilitate plastic flow, resulting in exaggerated surface roughness.

The results presented suggest that the electro-polished surface has a higher resistance against cracking damage than the mechanically polished surface under the applied heat loading conditions, and that only surface modification takes place in the electro-polished surface. Accordingly, it is worth making an attempt to install electro-polished PFMs in fusion devices and further investigate the interactions between plasma and W material with modified surface structures induced by cyclic transient thermal shocks.

Acknowledgments

We would like to express our gratitude to H. Greuner from IPP Garching for the support with HHF tests in GLADIS and valuable comments on this article. We would like to thank Dr Th Loewenhoff for the assistance with surface roughness measurements, and Dr P Swiatek for helpful discussions

during the course of preparing the manuscript. We thank Mr P Denner for the proof-reading of the manuscript. This work was supported by the National Magnetic Confinement Fusion Science Program of China under Grant 2013GB109004, and the National Nature Science Foundation of China under contract No. 51401012.

References

[1] Ueda Y., Coenen J.W., De Temmerman G., Doerner R.P., Linke J., Philipps V. and Tsitrone E. 2014 Research status and issues of tungsten plasma facing materials for ITER and beyond *Fusion Eng. Des.* **89** 901–6
[2] Federici G., Loarte A. and Strohmayer G. 2003 Assessment of erosion of the ITER divertor targets during type I ELMs *Plasma Phys. Control. Fusion* **45** 1523–47
[3] Kirk A., Lisgo S., Nardon E, Eich T., Herrmann A. and Kallenbach A. 2011 Physics of ELM power fluxes to plasma facing components and implications for ITER *J. Nucl. Mater.* **417** 481–6
[4] Makhlaj V. A. *et al* 2014 Plasma exposure of different tungsten grades with plasma accelerators under ITER-relevant conditions *Phys. Scr.* **T161** 014040
[5] Wirtz M., Linke J., Pintsuk G., Singheiser L. and Uytdenhouwen I. 2011 Comparison of the thermal shock performance of different tungsten grades and the influence of microstructure on the damage behavior *Phys. Scr.* **T145** 014058
[6] Hirai T., Pintsuk G. and Linke J. 2009 Cracking failure study of ITER-reference tungsten grade under single pulse thermal shock loads at elevated temperatures *J. Nucl. Mater.* **390–391** 751–4
[7] Pintsuk G., Kuhnlein W., Linke J. and Rodig M. 2007 Investigation of tungsten and beryllium behaviour under short transient events *Fusion Eng. Des.* **82** 1720–9
[8] Yuan Y., Greuner H., Boeswirth B., Krieger K., Luo G.-N., Xu H.Y., Fu B.Q., Li M. and Liu W. 2013 Recrystallization and grain growth behavior of rolled tungsten under VDE-like short pulse high heat flux loads *J. Nucl. Mater.* **433** 523–30
[9] Huber A. *et al* 2014 Investigation of the impact of transient heat loads applied by laser irradiation on ITER-grade tungsten *Phys. Scr.* **T159** 014005
[10] van Eden G.G., Morgan T.W., van der Meiden H.J., Matejicek J., Chraska T., Wirtz M. and De Temmerman G. 2014 The effect of high-flux H plasma exposure with simultaneous transient heat loads on tungsten surface damage and power handling *Nucl. Fusion* **54** 123010
[11] Yu J.H., De Temmerman G., Doerner R.P., Pitts R.A. and van den Berg M.A. 2015 The effect of transient temporal pulse shape on surface temperature and tungsten damage *Nucl. Fusion* **55** 093027
[12] Srinivasa-Murthy C., Wang D., Beaudoin S.P., Bibby T., Holland K. and Cale T.S. 1997 Stress distribution in chemical mechanical polishing *Thin Solid Films* **308–309** 533–7
[13] Malkin S. 1989 *Grinding Technology: Theory and Applications of Machining with Abrasives* (Chichester: Ellis Horwood)
[14] Pintsuk G., Prokhodtseva A. and Uytdenhouwen I. 2011 Thermal shock characterization of tungsten deformed in two orthogonal directions *J. Nucl. Mater.* **417** 481–6
[15] Pintsuk G. and Uytdenhouwen I. 2010 Thermo-mechanical and thermal shock characterization of potassium doped tungsten *Int. J. Refract. Met. Hard Mater.* **28** 661–8
[16] Greuner H., Boeswirth B., Boscary J. and McNeely P. 2007 High heat flux facility GLADIS: operational characteristics and results of W7-X pre-series target tests *J. Nucl. Mater.* **367–370** 1444–8
[17] Schiller S., Heisig U. and Panzer S. 1982 *Electron Beam Technology* (New York: Wiley)
[18] Du J., Yuan Y., Wirtz M., Linke J., Liu W. and Greuner H. 2015 FEM study of recrystallized tungsten under ELM-like heat loads *J. Nucl. Mater.* **463** 219–22
[19] Prior D.J. *et al* 1999 The application of electron backscatter diffraction and orientation contrast imaging in the SEM to textural problems in rocks *Am. Mineral.* **84** 1741–59
[20] Keshavarz Z. and Barnett M.R. 2006 EBSD analysis of deformation modes in Mg-3Al-1Zn *Scr. Mater.* **55** 915–18
[21] Huang X. and Liu Q. 1998 Determination of crystallographic and macroscopic orientation of planar structures in TEM *Ultramicroscopy* **74** 123–30
[22] Linke J. *et al* 2011 Performance of different tungsten grades under transient thermal loads *Nucl. Fusion* **51** 073017
[23] Wirtz M., Cempura G., Linke J., Pintsuk G. and Uytdenhouwen I. 2013 Thermal shock response of deformed and recrystallised tungsten *Fusion Eng. Des.* **88** 1768–72
[24] Seigle L.L. and Dickenson C.D. 1963 *Refractory Metals and Alloys II* (New York: Interscience)
[25] Uytdenhouwen I., Decréton M., Hirai T., Linke J., Pintsuk G. and Van Oost G. 2007 Influence of recrystallization on thermal shock resistance of various tungsten grades *J. Nucl. Mater.* **363–365** 1099–103
[26] Humphreys F.J. and Hatherly M. 2004 *Recrystallization and Related Annealing Phenomena* 2nd edn (Amsterdam: Elsevier)
[27] Wynick G.L. and Boehlert C.J. 2005 Use of electropolishing for enhanced metallic specimen preparation for electron backscatter diffraction analysis *Mater. Charact.* **55** 190–202
[28] Landolt D. 1987 Fundamental aspects of electropolishing *Electrochim. Acta* **32** 1–11
[29] Moore M.G. and Evans W.P. 1958 Mathematical correction for stress in removed layers in x-ray diffraction residual stress analysis *SAE Trans.* **66** 304–5
[30] Dümmer T., Lasalvia J.C., Ravichandran G. and Meyers M.A. 1998 Effect of strain rate on plastic flow and failure in polycrystalline tungsten *Acta Mater.* **46** 6267–90
[31] Murr L.E. and Esquivel E.V. 2004 Review observations of common microstructural issues associated with dynamic deformation phenomena: twins, microbands, grain size effects, shear bands and dynamic recrystallization *J. Mater. Sci.* **39** 1153–68
[32] Murr L.E. *et al* 1997 Shock-induced deformation twinning in tantalum *Acta mater* **45** 157–75
[33] Hsiung L.M. and Lassila D.H. 2000 Shock-induced deformation twinning and omega transformation in tantalum and tantalum-tungsten alloys *Acta Mater.* **48** 4851–65
[34] Pappu S. *et al* 2001 Deformation twins in oriented, columnar-grained tungsten rod ballistic penetrators *Mater. Sci. Eng.* A **298** 144–57
[35] Hall E.O. 1954 *Twinning* (London: Butterworths)
[36] Murr L.E. and Pizana C. 2007 Dynamic recrystallization: the dynamic deformation regime *Metall. Mater. Trans.* A **38** 2611–28
[37] Hines J. A., Vecchio K.S. and Ahzi S. 1998 A model for microstructure evolution in adiabatic shear bands *Metall. Mater. Trans.* A **29A** 191–203
[38] Trillo E.A., Esquivel E.V., Murr L.E. and Magness L.S. 2002 Dynamic recrystallization-induced flow phenomena in tungsten–tantalum (4%)[0 0 1] single-crystal rod ballistic penetrators *Mater. Charact.* **48** 407–21